A thermomechanically micromechanical modeling of prestressed concrete reinforced with shape memory alloys fibers

Yuval Freed ‡, Jacob Aboudi

Department of Solid Mechanics, Materials and Systems
Faculty of Engineering
Tel Aviv University, 69978 Ramat Aviv, ISRAEL

Rivka Gilat

Department of Civil Engineering
Faculty of Engineering
The College of JAS
44837 Ariel, ISRAEL

‡ Corresponding author: yuval@eng.tau.ac.il, tel: +972-3-6405581, fax: +972-3-6407617

Abstract.

Concrete is a very popular material in civil engineering, although it exhibits some limitations. The most crucial limitation is its low tensile strength, comparing to its compressive strength, which results from the propagation of micro-cracks. This may be prevented by using prestrained shape memory alloy wires that are embedded in the concrete matrix. Upon activation, these wires regain their original shape, and consequently, initial compressive stresses are transmitted to the concrete matrix. In this study, a thermomechanically micromechanical model of prestressed concrete reinforced by shape memory alloys fibers is presented and examined for different reinforcement aspects. It was found that there is a strong relation between the activation temperature deviation and the behavior of the prestressed concrete. The relation between the fibers volume fraction and the composite response and the effect of the shape of the reinforcing fibers and residual strain orientations are examined in details.

Keywords: Micromechanical Model, Thermomechanical coupling, Shape Memory Alloys, Prestressed Concrete, Effective properties, Averaging methods.

1. Introduction

Smart materials have received much attention in recent years, especially as a result of their various applications in actuators, smart structures, medical devices, space and aeronautics. Among these materials, shape memory alloys (SMA) exhibit extremely large, recoverable strains (of the order of 10%), resulting from the transformation between austenitic and martensitic phases. This transformation may be induced by a change: (1) in the applied stress (stress-induced transformation), (2) the temperature (temperature-induced transformation), and (3) a combination of the two. Although these materials are known for decades, they have not been used in the building industry until very recently, especially as passive and active vibration dampers, actuators, and sensors, as described in Janke et al. (2005).

Concrete is nowadays the most important material in the building industry. However, it is very weak in tension, comparing to its strength in compression. To overcome this problem, a prestressed concrete is usually used. Prestressed concrete is basically a plain concrete with reinforcement of steel, polymers or, in this case, shape memory alloys. The prestressing is usually introduced by tensioning the reinforcement in the concrete members. Consequently, initial compressive stresses are subjected to the concrete matrix; the application of permanent compressive stresses increases the apparent tensile strength of the material, since upon tension loading, the compressive stresses should be nullified first.

It is common to divide the methods of prestressing into two main groups, either *pre-tensioned* or *post-tensioned*. In a pre-tensioned system, the fibers are first tensioned up to a desired strain. Then, the concrete is cast around the stresses fibers. Past the concrete hardening, the fibers are released such that their residual strains are reduced while transferring (through interfacial shear) compression stresses to the concrete. In a post-tensioned system, the tension wires (placed in tubes which are embedded in the concrete) are tensioned by means of a jack bearing on the end face of the member and anchored by wedges or nuts. The compressive stresses are transmitted to the concrete through the end faces of the member.

There are several applications of prestressed concrete using shape memory alloys. Among these, Maji and Negret (1998) were the first to use strands made of SMA wires that were electrically actuated to induce deflection and failure in concrete beams. Following them, Deng et al. (2003, 2006) studied the effect of different properties, such as initial prestrain of SMA wires, modes of activating electrical current, and the actuation times, on the behavior of prestressed beam. Recently, El-Tawil and Ortega-Rosales (2004) and Sawaguchi et al. (2006) examined different experimental aspects of the post tensioning procedure. Finally, in case of thin walled members, and for small tension stresses, the use of SMA bars is not feasible anymore; for this purpose, SMA fibers may be embedded in the cement matrix, as suggested by Moser et al. (2006). Since in their study Moser et al. (2006) deal with fiber reinforced concrete, the tensioning procedure they used is a completely new concept. The already stretched SMA fibers

(with residual strains) are embedded in the concrete matrix in low temperature (that relates to the shape memory effect). Upon heating the composite, the SMA fibers regain their original shape, and compression stresses are transmitted to the concrete. This procedure of prestressing is referred to as *activation*.

There are numerous advantages of employing SMA fibers embedded in a concrete matrix. The use of SMA fibers is suitable for thin-walled structures and elements of various geometries (e.g., plates, shells and arcs) where the conventional prestressing approaches are not feasible or more complicated. Furthermore, in case of prestress decrease during the element's life period, the amount of prestressing can be increased at any given time. In addition, the activated SMA fibers may be used for retrofitting, repairing and strengthening structures. However, SMA fibers are still relatively expensive and possess a low Young's modulus as compared to steel.

Although the aforementioned investigations give a good qualitative picture of the essential phenomena of prestressed concrete, non of them suggested a methodology that can model the behavior of concrete reinforced and prestressed by shape memory alloys fibers. Hence, The main objective of this work is to develop a robust quantitative micromechanical procedure to obtain the effective mechanical properties and the behavior of a prestressed concrete reinforced with shape memory alloys fibers. This behavior is obtained for different shapes and volume fractions of the SMA fibers.

There are several micromechanical models that are capable to predict the macroscopic behavior of composite materials with embedded shape memory alloy fibers. Among these models, Boyd and Lagoudas (1994), Kawai et al. (1996), Carvelli and Taliercio (1999), Song et al. (1999), Kawai (2000), Gilat and Aboudi (2004, 2006), Marfia (2005) and Aboudi and Freed (2006). However, these models do not consider damage; hence, they are not suitable for the case of prestressed concrete. To properly investigate the behavior of prestressed concrete, the high fidelity generalized method of cells (HFGMC) micromechanical model, first presented by Aboudi et al. (2001, 2002, 2003) and reviewed by Aboudi (2004) is utilized. This model is capable to accurately predict the global (macroscopic) behavior of the composite by properly taking into account the detailed interaction between the various constituents.

As a first step, appropriate constitutive relations and energy equation of the SMA fibers need to be established. To this end, Panoskaltsis et al. (2004) presented a constitutive model for monolithic shape memory alloy. This model, briefly presented in Section 2, is used in the HFGMC micromechanical analysis as the 'fiber' in the composite. As the 'matrix', an appropriate constitutive model of concrete with progressive damage is used. This model, suggested by Tao and Phillips (2005), is described in Section 3. In Section 4, the HFGMC micromechanical analysis is applied for the prediction of the response of the inelastic SMA fibers and the concrete matrix. In Section 5, applications of the micromechanical model are presented. In this section, the behavior of prestressed concrete with shape memory alloy fibers for different shapes of fibers and volume fractions is examined, as well as the influence of the activation procedure. Summary and conclusions are given in Section 6.

2. Constitutive modeling of monolithic shape memory alloy

The modeling of the prestressed concrete with shape memory alloys fibers begins with choosing an appropriate constitutive model for the shape memory alloy fibers. In this study, the model proposed by Panoskaltsis et al. (2004) is considered. This model performs a general inelastic framework for the derivation of general three-dimensional thermomechanical constitutive equations for materials undergoing phase transformations. Its framework is based on the generalized plasticity theory and on some basic elements from the theory of continuum damage mechanics. In this section, this model is briefly described, although it is presented in slightly different notations. At the end of this section, the numerical integration scheme of the constitutive equations of the model is derived and explained in details.

As in most of SMA constitutive equations, this model considers only one internal variable. The internal scalar variable is denoted here by ξ, and it describes the martensite fraction. The general form of the transformation surface is taken as a von-Mises type surface, and given by

$$F(\boldsymbol{\sigma}, T) = \sqrt{3J_2} - CT, \tag{1}$$

where $\boldsymbol{\sigma}$ is the Cauchy stress tensor, $J_2 = \boldsymbol{s} : \boldsymbol{s}/2$ is the second invariant of the deviatoric stress tensor $\boldsymbol{s}$, C is a material property, T is the current temperature and the loading surface $F(\boldsymbol{\sigma}, T)$ is constant. The austenite to martensite transformation surface is given by

$$F_M(\boldsymbol{\sigma}, T) = \sqrt{3J_2} - C_M T, \tag{2}$$

where C_M is the slope of the one-dimensional stress-temperature diagram for martensite behavior. Moreover, introducing F_{M_s} and F_{M_f} as the loading surfaces at the beginning and the end of the transformation yields

$$\begin{aligned} F_{M_s}(\boldsymbol{\sigma}, T) &= \sqrt{3J_2} - C_M(T - M_s), \\ F_{M_f}(\boldsymbol{\sigma}, T) &= \sqrt{3J_2} - C_M(T - M_f), \end{aligned} \tag{3}$$

where M_s and M_f represents the martensite start and finish temperatures, respectively.

It may be easily shown that the product $F_{M_s}F_{M_f}$ is negative only during the austenite to martensite phase transformation. Hence, the expression for evolution of the martensite fraction during the forward transformation is given by

$$\dot{\xi} = -\frac{\langle -F_{M_s}F_{M_f} \rangle}{|F_{M_s}F_{M_f}|} \frac{1-\xi}{F_{M_f}} \langle \dot{F}_M \rangle, \tag{4}$$

where the dot above a quantity represents its increment and $\langle\cdot\rangle$ is the Macauley bracket, defined as $\langle x\rangle = (|x| + x)/2$. Evolution of the transformation strain tensor, or the so called 'flow rule', is given as

$$\dot{\boldsymbol{\epsilon}}^{tr} = \epsilon_L \dot{\xi} \boldsymbol{n}_{A\to M} \tag{5}$$

where ϵ_L is a material constant, which represents the maximum inelastic strain, and $\boldsymbol{n}_{A\to M}$ is the normal to the martensitic transformation surface, and defined by

$$\boldsymbol{n}_{A\to M} = \sqrt{\frac{3}{2}} \left(\frac{\boldsymbol{s}}{\bar{\sigma}} \right), \tag{6}$$

where the effective stress is given by

$$\bar{\sigma} = \sqrt{\frac{3}{2}\, \boldsymbol{s} : \boldsymbol{s}} \ . \tag{7}$$

Similarly, for the martensite to austenite transformation, the loading surfaces are defined as

$$\begin{aligned} F_A(\boldsymbol{\sigma}, T) \ &= \sqrt{3J_2} - C_A T, \\ F_{A_s}(\boldsymbol{\sigma}, T) &= \sqrt{3J_2} - C_A (T - A_s), \\ F_{A_f}(\boldsymbol{\sigma}, T) &= \sqrt{3J_2} - C_A (T - A_f), \end{aligned} \tag{8}$$

where C_A denotes the slope of the one-dimensional stress-temperature diagram for austenite behavior. Similar to the forward transformation, the product $F_{A_s} F_{A_f}$ is negative only for an evolving backward transformation. Evolution of the martensite fraction during the backward transformation is given by

$$\dot{\xi} = -\frac{\langle -F_{A_s} F_{A_f} \rangle}{|F_{A_s} F_{A_f}|} \frac{\xi}{F_{A_f}} \langle \dot{F}_A \rangle, \tag{9}$$

the flow rule of the backward transformation is

$$\dot{\boldsymbol{\epsilon}}^{tr} = \epsilon_L \dot{\xi} \boldsymbol{n}_{M\to A} \tag{10}$$

where

$$\boldsymbol{n}_{M\to A} = \sqrt{\frac{3}{2}} \left(\frac{\boldsymbol{\epsilon}^{tr}}{\bar{\epsilon}^{tr}} \right), \tag{11}$$

and the effective strain is given by

$$\bar{\epsilon}^{tr} = \sqrt{\frac{3}{2}\,\boldsymbol{\epsilon}^{tr} : \boldsymbol{\epsilon}^{tr}}\ . \tag{12}$$

Finally, The constitutive law of the SMA material is given by

$$\boldsymbol{\sigma} = \mathbf{C}(\xi) : (\boldsymbol{\epsilon} - \boldsymbol{\epsilon}^{tr}), \tag{13}$$

where $\mathbf{C}$ is the standard isotropic stiffness matrix but its components depend upon the internal variable ξ in the form

$$E = E_A + \xi^m \left(E_M - E_A\right) \tag{14}$$

and

$$\nu = \nu_A + \xi^m \left(\nu_M - \nu_A\right), \tag{15}$$

where E_A, E_M, ν_A and ν_M are the Young's moduli and Poisson ratios of austenite and martensite phases, respectively, and m is a positive material parameter, which controls the slope of the stress-strain curve.

The stress-strain behavior of the material may be separated into several different branches. It is clear that if $\dot{F}_A < 0$, backward transformation occurs, while forward transformation occurs if $\dot{F}_M > 0$. Since only one internal variable is considered, $\dot{F}_A = \dot{F}_M$; hence, only one phase transformation is active at any given time. Consequently, the forward and backward transformation may be decoupled into two separate criteria simply by defining

$$h_M = \frac{\langle -F_{M_s} F_{M_f} \rangle}{|F_{M_s} F_{M_f}|}, \qquad h_A = \frac{\langle -F_{A_s} F_{A_f} \rangle}{|F_{A_s} F_{A_f}|}. \tag{16}$$

For a forward transformation,

$$\begin{array}{ll} \text{if,}\ \ h_M = 0\ \ \text{then} & \text{elastic state} \\ \text{if}\ \ h_M = 1,\ \ \text{then} & \\ \quad \dot{F}_M < 0 & \text{elastic unloading} \\ \quad \dot{F}_M = 0 & \text{neutral loading} \\ \quad \dot{F}_M > 0 & \text{inelastic loading.} \end{array} \tag{17}$$

For a backward transformation,

$$\begin{array}{ll} \text{if}\ \ h_A = 0,\ \ \text{then} & \text{elastic state} \\ \text{if}\ \ h_A = 1,\ \ \text{then} & \\ \quad \dot{F}_A > 0 & \text{elastic unloading} \\ \quad \dot{F}_A = 0 & \text{neutral loading} \\ \quad \dot{F}_A < 0 & \text{inelastic loading.} \end{array} \tag{18}$$

From a computational point of view, the non-linear behavior of the model may be treated as an implicit time discrete strain driven problem. Accordingly, the time discrete equations of the model are integrated over a time interval $(t, t+\Delta t)$ using an implicit backward Euler scheme, which is unconditionally stable. In the following, the details of the computational procedure for the determination of the SMA response are presented.

During elastic deformation

$$\begin{aligned} \xi^{t+\Delta t} &= \xi^t, \\ \boldsymbol{\epsilon}^{tr,t+\Delta t} &= \boldsymbol{\epsilon}^{tr,t}, \end{aligned} \tag{19}$$

and the new stress state is determined using eq. (13). For both cases of inelastic loading, the discrete equations may be derived as

$$\begin{aligned} \xi^{t+\Delta t} &= \xi^t + \Delta\xi \\ \Delta\xi &= \frac{R_\xi^{t+\Delta t}}{f_f^{t+\Delta t}}\Delta F, \\ \Delta F &= \frac{3}{2}\frac{J_2^{t+\Delta t} - J_2^t}{\bar{\sigma}^{t+\Delta t}} - c(T^{t+\Delta t} - T^t), \\ J_2^{t+\Delta t} &= \frac{1}{2}\boldsymbol{s}^{t+\Delta t} : \boldsymbol{s}^{t+\Delta t}, \\ \boldsymbol{s}^{t+\Delta t} &= \frac{E^{t+\Delta t}}{1+\nu^{t+\Delta t}}\left(\boldsymbol{\epsilon}^{t+\Delta t} - \frac{1}{3}\boldsymbol{\epsilon}^{t+\Delta t} : \boldsymbol{I} - \boldsymbol{\epsilon}^{tr,t+\Delta t}\right), \\ \boldsymbol{\epsilon}^{tr,t+\Delta t} &= \boldsymbol{\epsilon}^{tr,t} + \Delta\xi\epsilon_L\boldsymbol{n}^{t+\Delta t}, \end{aligned} \tag{20}$$

where $\boldsymbol{I}$ is the identity matrix, $\boldsymbol{n}$ is given in eqs. (11) and (6) for backward and forward transformations, respectively,

$$R_\xi = 1 - \xi, \qquad f_f = -F_{M_f}, \qquad c = C_M, \tag{21}$$

for the case of a forward transformation, and

$$R_\xi = \xi, \qquad f_f = F_{A_f}, \qquad c = C_A, \tag{22}$$

for a backward transformation. The increment of the martensite fraction $\Delta\xi$ is obtained by solving the nonlinear equation

$$\Delta\xi - \frac{3}{2}\,\frac{R_\xi^{t+\Delta t}}{f_f^{t+\Delta t}}\,\frac{J_2^{t+\Delta t} - J_2^t}{\bar{\sigma}^{t+\Delta t}} - c(T^{t+\Delta t} - T^t) = 0\,, \tag{23}$$

and the new stress state may be determined using eqs. (20) and (13).

The response of the material during an isothermal strain-driven uniaxial loading-unloading test is shown in Figs. 1a and 1b for the cases when $M_s < T < A_s$ and

$A_s < T < A_f$, respectively. In the analyses, Young's moduli are taken as $E_M = 500$ MPa and $E_A = 1500$ MPa, the Poisson's ratios $\nu_A = \nu_M = 0.3$, the transformation temperatures are $M_s = 70°\text{C}$, $M_f = 10°\text{C}$, $A_s = 90°\text{C}$, $A_f = 130°\text{C}$, the slopes $C_M = C_A = 1$ MPa/°C, $\epsilon_L = 0.1$ and $m = 1$. These results agree exactly with those of Panoskaltsis et al. (2004).

3. Constitutive modeling of plain concrete

In this study, the constitutive model of plain concrete suggested by Tao and Phillips (2005), was chosen and implemented. This model presents a three-dimensional analysis of concrete, with a feature of simplicity and avoidance of convergence problems, often observed in strain softening plasticity. This model describes the strain softening of a plain concrete in a framework of a continuum damage mechanics, with a weighted damage parameter and a damage multiplier that eliminates potential convergence problems and reduce the effect of hydrostatic pressure on damage. It may be noted that only a brief derivation of the model is given here. For further details, the reader is directed to Tao and Phillips (2005).

Under isothermal conditions, the Helmholtz free energy may be written as

$$A = \frac{1}{2}\boldsymbol{\epsilon} : \mathbf{K} : \boldsymbol{\epsilon}, \tag{24}$$

where $\mathbf{K}$ is the fourth-order stiffness tensor of the material, and $\boldsymbol{\epsilon}$ is the strain tensor. Since experimental observations suggest that the failure of concrete is different for hydrostatic and deviatoric loadings, the above potential may be decoupled as

$$A = \frac{1}{2}(1 - D)\,\boldsymbol{\epsilon} : \mathbf{K}^0 : \boldsymbol{\epsilon} + \frac{(1 - \beta)\,D}{2}\epsilon_m^2 \mathbf{I} : \mathbf{K}^0 : \mathbf{I}, \tag{25}$$

where the stiffness degradation induced by material damage $\mathbf{K} = (1 - D)\mathbf{K}^0$ is considered, $\epsilon_m = \boldsymbol{\epsilon} : \mathbf{I}/3$ is the mean strain, and β denotes for a damage multiplier that reduces the influence of the hydrostatic loading as

$$\beta = 1 - \frac{1}{1 + cY e^{-dY}} \tag{26}$$

with c and d as material constants and Y as a thermodynamic force. Finally, D is a combined tension/compression damage parameter

$$D = \frac{\sum \sigma_p^+ D_t + \sum |\sigma_p^-| D_c}{\sum |\sigma_p|}, \tag{27}$$

where σ_p^+ and σ_p^- are the positive and negative parts of the principal stress tensor, respectively, $\sum |\sigma_p|$ is the sum of the absolute values of the principal stresses, and D_t and D_c are scalars that denotes for the damage in tension and compression, respectively.

It should be noted that according to eq. (27), the damage in tension does not induce a damage in compression.

The thermodynamic force Y may be separated to Y_t for tension and Y_c for compression as

$$Y_t = \frac{\partial A}{\partial D_t} = \frac{\sum \sigma_p^+}{2\sum |\sigma_p|} \left(\boldsymbol{\epsilon} : \mathbf{K}^0 : \boldsymbol{\epsilon} - (1-\beta)\epsilon_m^2 \mathbf{I} : \mathbf{K}^0 : \mathbf{I} \right), \tag{28}$$

$$Y_c = \frac{\partial A}{\partial D_c} = \frac{\sum \sigma_p^-}{2\sum |\sigma_p|} \left(\boldsymbol{\epsilon} : \mathbf{K}^0 : \boldsymbol{\epsilon} - (1-\beta)\epsilon_m^2 \mathbf{I} : \mathbf{K}^0 : \mathbf{I} \right), \tag{29}$$

and

$$\boldsymbol{\sigma} = \frac{\partial A}{\partial \boldsymbol{\epsilon}} = (1-D)\mathbf{K}^0 : \boldsymbol{\epsilon} + \frac{(1-\beta)D\epsilon_m}{3}(\mathbf{I} : \mathbf{K}^0 : \mathbf{I})\mathbf{I} \tag{30}$$

Since no plastic strain is taken into account in this model, the material tangent and secant moduli may be determined as

$$\mathbf{K}_t = (1-D)\mathbf{K}^0 + \frac{(1-\beta)D}{9}(\mathbf{I} : \mathbf{K}^0 : \mathbf{I})\mathbf{I} \tag{31}$$

Finally, limits functions for tension and compression are given by

$$f_t(Y_t, D_t) = Y_t - Z_t = 0 \tag{32}$$

$$f_c(Y_c, D_c) = Y_c - Z_c = 0 \tag{33}$$

where the softening parameters Z_t and Z_c are expressed as

$$Z_t = Y_t^0 + \frac{1}{a_t}\left(\frac{D_t}{1-D_t}\right)^{\frac{1}{b_t}} \tag{34}$$

$$Z_c = Y_c^0 + \frac{1}{a_c}\left(\frac{D_c}{1-D_c}\right)^{\frac{1}{b_c}}, \tag{35}$$

in which parameters a_t and b_t are determined from a simple uniaxial tensile test, while a_c and b_c are determined from a uniaxial compression test. The initial values of damage energy release rates, Y_t^0 and Y_c^0, are material constants, which denotes for the onset of the damage in tension and compression, respectively.

The response of concrete in tension and compression is illustrated in Figs. 2a and 2b, respectively. In the analyses, Young's modulus was taken as $E = 31.8$ GPa, with $\nu = 0.18$, $a_t = 7000$ MPa^{-1}, $b_t = 1.1$, $a_c = 29$ MPa^{-1}, $b_c = 0.94$, $Y_t^0 = 1.9 \times 10^{-4}$ MPa, $Y_c^0 = 3 \times 10^{-4}$ MPa, $c = 2$ MPa^{-1} and $d = 0.7$ MPa^{-1}. The results are in excellent agreement with those of Tao and Phillips (2005).

4. Micromechanical analysis

The micromechanical model employed to predict the effective thermoelastic properties and inelastic response of multiphase composites is referred to as the the "high-fidelity generalized method of cells" (HFGMC) and has been fully described in Aboudi et al. (2001, 2002, 2003). This model is based on a homogenization technique of composites with periodic microstructure as shown in Fig. 3. The repeating unit cell of such a composite is divided into arbitrary number of rectangular subcells, labeled by the indices (β, γ), each of which may contain a distinct homogeneous material. The dimensions of the subcell along the 2 and 3 axes are denoted by h_β and l_γ, respectively. In the present two-dimensional case of continuous fibers, a local coordinate system $(\bar{y}_2^{(\beta)}, \bar{y}_3^{(\gamma)})$ is introduced in each subcell whose origin is located at its center.

The local (subcell) constitutive equation of the material which, in general, is assumed to be thermo-inelastic, is given by

$$\boldsymbol{\sigma}^{(\beta\gamma)} = \mathbf{C}^{(\beta\gamma)} : (\boldsymbol{\epsilon}^{(\beta\gamma)} - \boldsymbol{\epsilon}^{\mathbf{I}(\beta\gamma)} - \boldsymbol{\epsilon}^{\mathbf{T}(\beta\gamma)}) \tag{36}$$

where $\boldsymbol{\sigma}^{(\beta\gamma)}$ is the stress tensor in subcell (β, γ), $\mathbf{C}^{(\beta\gamma)}$ is the stiffness tensor of the material in the subcell and $\boldsymbol{\epsilon}^{(\beta\gamma)}, \boldsymbol{\epsilon}^{I(\beta\gamma)}, \boldsymbol{\epsilon}^{T(\beta\gamma)}$ are the total, inelastic and thermal strain tensors, respectively. It should be noted that the stiffness tensor $\mathbf{C}^{(\beta\gamma)}$ varies as the deformation develops. This results from the fact that for the SMA fibers, the elastic moduli change with the internal variable ξ (see eqs. 14 and 15) whereas for the concrete matrix its moduli change with the progress of damage (see eq. 27). The inelastic strain increments at the various locations within the subcell are calculated using the flow rules given in eqs. (5) and (10) for forward and backward transformation of the shape memory alloy material, while the thermal strains are given in terms of the coefficients of thermal expansion multiplied by the temperature deviation from a reference temperature.

The basic assumption in HFGMC is that the displacement vector in each subcell is given by the quadratic form

$$\begin{aligned}\mathbf{u}^{(\beta\gamma)} = {} & \bar{\boldsymbol{\epsilon}} \cdot \mathbf{x} + \mathbf{W}_{(00)}^{(\beta\gamma)} + \bar{y}_2^{(\beta)} \mathbf{W}_{(10)}^{(\beta\gamma)} + \bar{y}_3^{(\gamma)} \mathbf{W}_{(01)}^{(\beta\gamma)} \\ & + \frac{1}{2}(3\bar{y}_2^{(\beta)2} - \frac{h_\beta^2}{4}) \mathbf{W}_{(20)}^{(\beta\gamma)} + \frac{1}{2}(3\bar{y}_3^{(\gamma)2} - \frac{l_\gamma^2}{4}) \mathbf{W}_{(02)}^{(\beta\gamma)}\end{aligned} \tag{37}$$

where $\bar{\boldsymbol{\epsilon}}$ is the applied (external) strain and the unknown terms $\mathbf{W}_{(mn)}^{(\beta\gamma)}$ must be determined from the fulfillment of the equilibrium equations, the periodic boundary conditions and the interfacial continuity conditions of displacements and traction between subcells, see Aboudi et al. (2001) for more details. A principal ingredient in the present micromechanical analysis is that all these conditions are imposed in the average (integral) sense.

As a result of the imposition of these conditions a linear system of algebraic equations is obtained which can be represented in the following form

$$\mathbf{KU} = \mathbf{f} + \mathbf{g} \tag{38}$$

where the matrix $\mathbf{K}$ contains information on the current material properties of the subcell and its dimensions, $\mathbf{U}$ contains the unknown terms $\mathbf{W}_{(mn)}^{(\beta\gamma)}$ in the displacement expansion, eq. (37), the $\mathbf{f}$ vector contains information on the externally applied strain and thermal effects, and $\mathbf{g}$ contains the inelastic effects expressed by integrals of inelastic strains.

Once eq. (38) is solved, the local stress and strain fields throughout the repeating unit cell can be determined. This is accomplished by the establishment of the strain concentration tensor $\mathbf{A}^{(\beta\gamma)}$ of the subcell which relates the local field to the externally applied one (see Aboudi, 2004, for details). As a result, the micromechanically established constitutive equations that govern the overall (global) behavior of the multiphase material can be represented in the form

$$\bar{\boldsymbol{\sigma}} = \mathbf{C}^* : \ (\bar{\boldsymbol{\epsilon}} - \bar{\boldsymbol{\epsilon}}^I + \bar{\boldsymbol{\epsilon}}^T) \tag{39}$$

In this equation, $\bar{\boldsymbol{\sigma}}$ is the average stress in the composite, $\mathbf{C}^*$ is its current effective elastic stiffness tensor, and $\bar{\boldsymbol{\epsilon}}, \bar{\boldsymbol{\epsilon}}^I$ and $\bar{\boldsymbol{\epsilon}}^T$ are the overall total, inelastic and thermal strain tensors, respectively. The latter is given by the effective coefficients of thermal expansion multiplied by the temperature increment. A notable feature of the present model is that it provides closed-form expressions for $\mathbf{C}^*$, $\bar{\boldsymbol{\epsilon}}^I$ and $\bar{\boldsymbol{\epsilon}}^T$ (namely for the effective coefficients of thermal expansion) in terms of the geometry of the repeating unit cell and the current material properties of its constituents. These closed-form expressions have been summarized and presented in Aboudi (2004).

It should be noted that the present model is semi analytical and differs in several aspects from the finite element procedure, as discussed in Aboudi et al. (2002, 2003) and Aboudi (2004). In particular, the present micromechanical analysis can be used to analyze a composite structure. It should be noted that a finite element analysis may be a relatively complicated procedure to obtain the macroscopic inelastic behavior of the reinforced concrete, since several sets of numerical analyses are needed. However, using a finite element method for the establishment of the macroscopic constitutive equations of the SMA/concrete, and employing them subsequently as a consistent tangent modulus in another structural analysis (possibly in conjunction with a finite element one) appears to be a formidable task.

5. Problem formulation and results

Consider a unidirectional composite that consists of a concrete matrix reinforced by uniformly distributed SMA fibers which are oriented in the x_1 axial direction, see Fig. 4a. The present analyses were carried out for the case of a uniaxial stress loading in which the composite is subjected to an external strain in the axial direction while

keeping all other stress components equal to zero. To this end, the thermomechanically micromechanical model was examined in several aspects. First, the effect of the shape of the fibers was examined both for a case of a mismatch between the coefficients of thermal expansion of the SMA fibers and the concrete matrix, and for a case of zero thermal expansions. Next, the effects of the activation (as explained in the following) and the fibers volume fraction were examined. Finally, the transverse response due to axial loading was examined in terms of activation and volume fraction. Furthermore, the preferred orientation of the SMA fibers is examined as well. The material properties of the concrete and the SMA fibers are given in Tables 1 and 2, respectively. These properties are taken from Tao and Phillips (2005) for concrete, and Panoskaltsis et al. (2004) for SMA.

In order to model the prestressed concrete, the shape memory effect was utilized. With this phenomenon, when the initial temperature of the SMA is lower than the austenite start temperature A_s, residual strains are generated after loading-unloading cycle. These strains may be recovered simply by heating to a temperature above the austenite final temperature A_f. Consequently, the activation process was modeled as follow. First, the SMA fibers were subjected to a loading-unloading cycle with a temperature below A_s. As a result, residual strains $\boldsymbol{\epsilon}^0$ (given in Table 1) were generated. These fibers are embedded in the concrete matrix. Upon subsequent heating of the composite, these strains were recovered, and compressive stresses were transmitted to the concrete matrix. By employing the HFGMC, the algorithm for the prestessing process is as follow:

(i) Fill all subcells with SMA.

(ii) Load and unload the SMA material to get the residual strains, $\boldsymbol{\epsilon}^0$, and the corresponding internal variables.

(iii) Fill the subcells of the repeating unit cell according to the given composite configuration.

(iv) Assign zeros for the initial strains and internal variables of the matrix subcells.

(v) The initial global strain, $\bar{\boldsymbol{\epsilon}}$, is taken to be zero.

(vi) In the subcells that are filled with SMA fiber, the relation $\bar{\boldsymbol{\epsilon}}^{(\beta\gamma)} = \boldsymbol{\epsilon}^0 + \boldsymbol{A}\bar{\boldsymbol{\epsilon}}$ is used, where $\mathbf{A}^{(\beta\gamma)}$ is the strain concentration tensor of the subcell which is provided by the micromechanical analysis, while $\boldsymbol{\epsilon}^0$ and the initial value of the internal variable are those of step (ii). It should be noted that for the micromechanical local-global relations, only the portion $\bar{\boldsymbol{\epsilon}}^{(\beta\gamma)} - \boldsymbol{\epsilon}^0$ is considered.

5.1. Effect of the shape of the fibers on the behavior of the prestressed concrete

In this subsection, the effect of the shape of the fibers on the behavior of the prestressed concrete was examined. To this end, 64 subcells in a configuration of 8×8 were considered. Fibers with three different shapes of cross-section were examined: circle, ring, and U-shaped, as illustrated in Fig. 4b-d. The reader may recall that the volume

fraction of the fiber is relatively small (for example, in Moser et al., 2005, the fiber volume fraction was 1.2 %), and these figures just show the shape of the fiber qualitatively.

The analyses were carried out for two cases. In the first one, no thermal effects were considered (i.e., the thermal coefficient of expansion is taken as zero for both SMA and concrete constituents). In the second case, non-zero thermal expansions (as given in Tables 1 and 2) were considered. With these two cases, the effect of activation process may be examined in the absence and presence of thermal expansion. In all cases, the activation temperature deviation was taken as $\Delta T = 40°C$ with fibers volume fraction of $v_f = 1\%$. The results are illustrated in Fig. 5.

In Fig 5a, stress-strain curves were obtained for different shapes of fibers, with zero thermal expansions. Hence, the temperature deviation ΔT contributes only to the activation of the fibers (with all thermal strains equal to zero). From this graph, it may be observed that all fiber shapes exhibited a better performance as compared to the plain concrete. In all cases, both the peak of the stress, and the response in the damaged region exhibited an increase in the stress level. This increase was found to be approximately 400% to 530% for the different shapes with respect to a concrete with no prestressing. In particular, it was found that the ring shape, illustrated in Fig.4c, is the preferred shape of reinforcement. However, it is interesting to observe that once the temperature deviation ΔT is incorporated with the thermal expansion of the composite's phases, the difference between the responses of the fiber shapes is negligible, as shown in Fig. 5b. Nevertheless, the prestressed composite still exhibits a better performance in the damaged region, showing an increase of up to 75% in the stress level. To explain this phenomenon, the reader may recall that the compressive stresses in the concrete result from the recovery of the residual strains in the SMA fibers. If the thermal expansion of the composite is considered as well, the thermal strains reduce the effect of the SMA residual strains on the overall composite, since the volume fraction of the SMA fibers is relatively small. It may be shown that for relatively high values of v_f, the prestressed concrete exhibits an increase in the stress level.

5.2. Effect of activation and volume fraction on the behavior of prestressed concrete

As mentioned in the previous subsection, the induced temperature has a significant effect on the behavior of the prestressed concrete. In this subsection, this effect is examined for a range of activation temperature deviations. From Table 1, it is observed that a temperature deviation of $\Delta T = 40°\text{C}$ is sufficient for a full recovery of a monolithic SMA (since $A_f - A_s = 40°\text{C}$). However, since the fibers are embedded in the concrete matrix, there are obviously internal forces between the two phases which change the transformation temperatures. Consequently, $\Delta T = 40°\text{C}$ is not the optimal temperature deviation in the sense that full recovery is not necessarily achieved.

In Fig. 6a, the behavior of the prestressed concrete at different activation temperature deviations is shown. In all cases, 9 subcells in a configuration of 3×3, with fibers volume fraction of 1%, and non-zero thermal expansions were considered. In

these analyses, It is clear that all activations exhibit an increase in the stress level at the damaged region. However, it may be observed that a better prestressing is achieved with the increase of the temperature deviation ΔT, from 33% for $\Delta T = 10°\text{C}$, up to 750% for $\Delta T = 100°\text{C}$.

Furthermore, the relation between the activation temperature deviation and the martensite fraction ξ was examined, as illustrated in Fig. 6b. It may be noted that the martensite fraction ξ represents the amount of residual strains, in which $\xi = 1$ denotes the fully transformed martensite, which corresponds to the values of the residual strains $\epsilon^0_{11}, \epsilon^0_{22}, \epsilon^0_{33}$ given in Table 1. In this figure, $\bar{\sigma}_{ss}$ denotes for the steady state axial stress in the damaged region, while $\bar{\sigma}_{np}$ denotes for the steady state axial stress for SMA/concrete composite with no prestressing. The behavior exhibited by these curves is similar to that of Fig. 6a. Namely, a better prestressing is achieved with the increase of the temperature deviation. However, it is observed that the same level of prestressing is reached for different values of martensite fraction ξ. For instance, in the case of $\Delta T = 10°\text{C}$, the same level of prestressing is achieved even for low values of martensite fraction ($\xi \cong 0.1$), whereas in the case of $\Delta T = 100°\text{C}$, steady state is reached only for $\xi \cong 0.9$.

Although it seems tempting to use the highest temperature deviation for the activation process, the reader may recall that the entire composite material is subjected to this temperature deviation, and not only the SMA fibers. However, properties of concrete are altered significantly by exposure to high temperatures, mostly in terms of reduced stiffness and strength. Hence, the prestressing may be negligible, as compared to the damage degradation caused by the appearance of new micro-cracks in the heated concrete. Nevertheless, a proper choice of the concrete and the SMA fibers may allow the use of a high temperature activation. It should be noted that the effect of the mismatch between the coefficients of thermal expansion of the SMA and the concrete phases was examined within a range of $\alpha_{SMA}/\alpha_{concrete} = 0.5 - 2$. This effect turns out to be negligible.

Next, the effect of the fibers volume fraction on the stress-strain curve of the prestressed concrete is examined. Following the experimental setup of Moser et al. (2005), volume fractions of 0%, 0.5%, 1%, 1.5% and 2% were considered. In all cases, a temperature deviation of $\Delta T = 40°\text{C}$ was taken, and non-zero thermal expansions were considered. Nine subcells in a configuration of 3×3 were employed in the modeling.

In Fig. 7, the stress-strain responses of composites with different volume fractions are illustrated. It was found that the stress level in the damaged region increases with the increase of the volume fraction. That is due to the fact that more compressive stresses are transmitted to the concrete as the fiber volume fraction increases. It may be noted that with a higher volume fraction, the mechanical behavior of the SMA fiber contributes significantly to the overall behavior. However, due to the relatively low stress level threshold of the undamaged concrete, the overall stress level in the composite reduces to a relatively low level. Consequently, the SMA fiber cannot produce any new transformation strains, and the increase in the stress level of the prestressed concrete is mainly attributed to the activation process.

5.3. The transverse response of the prestressed concrete

It is interesting to study the resulting transverse response of the prestressed concrete due to axial loading. This response was examined by means of activation temperature deviations, and for a range of fiber volume fractions. In all cases, 9 subcells in a 3×3 configuration were considered.

In Fig. 8, the effect of the activation process on the transverse response is illustrated. In all cases, the fiber volume fraction was taken as $v_f = 1\%$, and non-zero thermal expansions were considered. This graph describes the evolution of the overall Poisson's ratio in terms of $-\bar{\epsilon}_{22}/\bar{\epsilon}_{11}$. For the case of SMA/concrete composite with no activation, this ratio starts with $-\bar{\epsilon}_{22}/\bar{\epsilon}_{11} = 0.1801$, which is the effective Poisson's ratio of the composite. This ratio varies rapidly due to the concrete softening, until it reaches a limit of $-\bar{\epsilon}_{22}/\bar{\epsilon}_{11} = 0.4977$, which is almost the incompressible limit of $\nu = 0.5$. It does not reaches the exact incompressible limit since there is still an amount of 1% of SMA fibers. In the case of activation, the initial ratio $-\bar{\epsilon}_{22}/\bar{\epsilon}_{11}$ starts with a negative value. This is due to the fact that the starting point of the applied axial loading follows the heating activation process. During this prestressing procedure, the applied temperature deviation causes almost a free stress expansion of the composite. Consequently, this expansion is characterized by $\bar{\epsilon}_{11} > 0$ and $\bar{\epsilon}_{22} > 0$. Upon loading, the ratio $-\bar{\epsilon}_{22}/\bar{\epsilon}_{11}$ varies and become positive, until it reaches a steady-state limit, in the region of softening concrete. It should be emphasized that the ratio $-\bar{\epsilon}_{22}/\bar{\epsilon}_{11}$ does not represent the current value of the Poisson's ratio of the composite.

It is observed from this figure that the ratio $-\bar{\epsilon}_{22}/\bar{\epsilon}_{11}$ increases upon loading, and it grows rapidly for relatively small temperature deviations. The initial value of $-\bar{\epsilon}_{22}/\bar{\epsilon}_{11}$ changes with the imposed temperature deviation, so that for increasing ΔT, the initial starting ratio is more negative. In all cases, the graphs reaches a steady state values of $-\bar{\epsilon}_{22}/\bar{\epsilon}_{11} = 0.4977, 0.4651, 0.4040, 0.3495$ and 0.2742 for temperature deviations of $\Delta T = 0^\circ, 10^\circ, 30^\circ, 50^\circ, 80^\circ$ and 100°, respectively.

The relation between the fiber volume fractions and the transverse response of the prestressed concrete caused by axial loading is shown in Fig. 9. Volume fractions of $0\%, 0.5\%, 1\%, 1.5\%$ and 2% were considered. In all cases, the temperature deviation for the activation process was taken as $\Delta T = 40°\text{C}$. For the case of plain concrete ($v_f = 0\%$), the initial value of the ratio $-\bar{\epsilon}_{22}/\bar{\epsilon}_{11}$ was exactly 0.18, which is identical to the Poisson's ratio of the concrete. For a damaged concrete, this ratio reached the limit value of $-\bar{\epsilon}_{22}/\bar{\epsilon}_{11} = 0.5$, which is the incompressibility limit. However, for the case of a prestressed concrete, the initial value of the ratio $-\bar{\epsilon}_{22}/\bar{\epsilon}_{11}$ was found to be negative, with an increasing value until it became positive. It is interesting that only slight differences were observed between the transverse responses for different fiber volume fractions. Consequently, it seems that the transverse response is mainly related to the activation temperature deviation, and not to the fiber volume fraction.

5.4. Effect of residual strains orientation on the prestressed concrete

Finally, the effect of the residual strains orientation on the prestressed concrete was examined. To this end, a hollow square -shape SMA fiber was considered. Residual strains ϵ^0_{11}, ϵ^0_{22} and ϵ^0_{33} which are given in Table 1, were employed in the axial and transverse directions of the fibers. These strains were imposed in all principal directions, with values of $[\epsilon_0, -\epsilon_0/2, -\epsilon_0/2]$, where the value ϵ_0 is prescribed in the axial or transverse direction, as shown in Fig. 10. In all cases, 64 subcells in a configuration of 8×8 were considered, with a fiber volume fraction of 1% and an activation temperature deviation of $\Delta T = 40°\text{C}$. Non-zero thermal expansions were considered for both concrete and SMA.

In Fig. 10, the stress-strain response due to axial loading is presented. As a reference, a SMA/concrete composite with no prestressing was used. As mentioned above, the different orientations of the residual strains are described in the figure, and labeled by (1) for positive transverse residual strains, (2) for negative transverse residual strains and (3) for positive axial residual strains. These strains subsequently released during the activation process, and consequently, stresses are transmitted to the concrete matrix.

Observing Fig. 10, it is clear that the case of positive transverse residual strains (case 1) reduces the strength of the composite. This results from the fact that upon heating, the SMA fiber regains its original shape, which corresponds to tensile stresses in the concrete matrix. On the other hand, in the case of negative transverse residual strains (case 2), an opposite phenomenon occurs; upon activation, the strength of the prestressed concrete increases significantly. This is due to compressive stresses that are transmitted to the concrete matrix. In the case of axial residual strains (case 3), an increase in the strength of the composite is observed. It may be noted that although ϵ_0 is the dominant residual strain, there are still two other components of residual strains $-\epsilon_0/2$ in the other principal directions. Consequently, in the latter case of an axial orientation, negative residual strains are still observed in the transverse direction, although they are of significantly lower values. Hence, prestressing still occur in the concrete. To conclude this discussion, it appears that case 2 is the best choice for a residual strain orientation in the fiber.

6. Discussion and conclusion

In this study, a thermomechanically micromechanical model for concrete prestressed by shape memory alloys fibers was derived and examined. This model accounts for the initial residual strains before the prestressing procedure, and the generated compressive stresses after the activation process. It is capable to model the degradation of the composite stiffness due to concrete softening, and consequently, describes the current macroscopic stress-strain relation. With the aid of this model, the relations between a prestressed fiber-reinforced concrete and its properties were investigated.

The SMA fiber-reinforced prestressed concrete was examined in several aspects. First, the effect of the shape of the fiber's cross-section was considered for circled, ring and U-shaped fibers. It was found that the shape of the fibers does not affect the composite behavior significantly, as long as non-zero thermal expansions are considered. However, if the thermal expansions are ignored, then the shape of the fibers is rather important. It was found that the 'ring' shape exhibits the best results, with a maximum increase of 530% in the stress level.

The effect of the activation process itself was examined as well. It was found that the stress level in the damaged region of the composite increases with the temperature deviation. This results from a higher level of compressive stresses in the concrete matrix. Moreover, the transverse response is strongly dependent upon the activation process.

Finally, the relation between the fiber volume fraction and the composite response was examined. It was found that an increase in the volume fraction corresponds to an increase in the stress level of the prestressed concrete. This is due to the higher compressive stresses that are generated and transmitted to the concrete matrix. However, the dependence of the transverse response on the fiber volume fraction is negligible, as compared to its dependence on the activation temperature deviation.

It may be noted that in the present paper a perfect bonding between the SMA fibers and the concrete was assumed. In practice, it is possible that the bond is initially imperfect and it further deteriorates as the loading increases. Indeed, it was shown by Maji and Negret (1998) that the bond between concrete and SMA fibers is relatively weak as compared to the bond with steel fibers. The SMA/concrete bond can be improved by creating a mechanical interlock, either by using four-wires strands (Maji and Negret, 1998) or by shaping the SMA wires into loops or star shapes (Moser et al., 2005). It should be noted that damage effects and their analysis have been already incorporated with the present micromechanical model by Bednarcyk et al. (2004), for the case of a metal matrix composite. This analysis of imperfect bonding evolution can be also employed in the present system of SMA/concrete.

As a future work, this micromechanical model may be applied with a more general concrete model, that incorporates inelastic strains. With this model, the fatigue and creep of the SMA prestressed concrete can be determined. Furthermore, a generalization of this model to three dimensions (short fiber composite) may assist in modeling more complex reinforcements of prestressed concrete. In addition, our future research will employ a structural analysis in which the established macroscopic constitutive equations will be used as a 'driver' to predict the response of a composite structure (e.g. a beam) that consists of a prestressed concrete matrix reinforced by SMA fibers.

References

Aboudi J., Pindera M-J. and Arnold S.M., Linear thermoelastic higher-order theory for periodic multiphase materials. *Journal of Applied Mechanics*, 68: 697-707 (2001).

Aboudi J., Pindera M.-J. and Arnold S.M., High-fidelity generalized method of cells for inelastic periodic multiphase materials. NASA TM-2002-211469 (2002).

Aboudi J., Pindera M.-J. and Arnold S.M., Higher-order theory for periodic multiphase materials with inelastic phases. *International Journal of Plasticity*, 19: 805-847 (2003).

Aboudi J., The generalized method of cells and high-fidelity generalized method of cells micromechanical models - a review. *Mechanics of Advanced Materials and Structures*, 11: 329-366 (2004).

Aboudi J. and Freed Y., Two-way thermomechanically coupled micromechanical analysis of shape memory alloy composites. *Journal of Mechanics of Materials and Structures*, 1: 937-955 (2006).

Bednarcyk B.A., Arnold S.M. Aboudi, J. and Pindera M-J., Local field effects in titanium matrix composites subject to fiber-matrix debonding. *International Journal of Plasticity*, 20: 1707-1737 (2004).

Boyd J.G. and Lagoudas D.C., Thermomechanical response of shape memory composites. *Journal of Intelligent Materials, Systems and Structures*, 5: 333-346 (1994).

Carvelli V. and Taliercio A., Micromechanical model for the analysis of unidirectional elasto-plastic composites subjected to 3D stresses. *Mechanics Research Communications*, 26: 547-553 (1999).

Deng Z.C., Li Q.B., Jiu A. and Li L., Behavior of concrete driven by uniaxially embedded shape memory alloy actuators. *Journal of Engineering Mechanics*, 129: 697-703 (2003).

Deng Z.C., Li Q.B. and Sun H.J., Behavior of concrete beam with embedded shape memory alloy wires. *Engineering Structures*, 28: 1691-1697 (2006).

El-Tawil S. and Ortega-Rosales J., Prestressing concrete using shape memory alloy tendons. *ACI Structural Journal* , 101: 846-851 (2004).

Gilat R. and Aboudi J., Dynamic response of active composite plates: shape memory alloy fibers in polymeric/metallic matrices. *International Journal of Solids and Structures*, 41: 5717-5731 (2004).

Gilat R. and Aboudi J., Thermal buckling of activated shape memory reinforced laminated plates. *Smart Materials and Structures*, 15: 829-838 (2006).

Janke L., Czaderski C., Motavalli M. and Ruth J., Applications of shape memory alloys in civil engineering structures - Overview, limits and new ideas. *Materials and Structures*, 38:578-592 (2005).

Kawai M., Ogawa H., Baburaj V. and Koga T., Micromechanical analysis for hysteretic behavior of unidirectional TiNi SMA Fiber Composite. *Journal of Intelligent Materials, Systems and Structures*, 10: 14-28 (1996).

Kawai M., Effects of matrix inelasticity on the overall hysteretic behavior of TiNi-SMA fiber composites. *International Journal of Plasticity*, 16: 263-282 (2000).

Maji A.K. and Negret I., Smart prestressing with shape-memory alloy. *Journal of Engineering Mechanics*, 124: 1121-1128 (1998).

Marfia S., Micro-macro analysis of shape memory alloy composites. *International Journal of Solids and Structures*, 42: 3677-3699 (2005).

Moser K., Bergamini A., Christen R. and Czaderski C., Feasibility of concrete prestressed by shape memory alloy short fibers. *Materials and Structures*, 38: 593-600 (2005).

Panoskaltsis V.P., Bahuguna S. and Soldatos D., On the thermomechanical modeling of shape memory alloys. *International Journal of Non-Linear Mechanics*, 39: 709-722 (2004).

Sawaguchi T., Kikuchi T., Ogawa K., Kajiwara S., Ikeo Y., Kojima M. and Ogawa T., Development of prestressed concrete using Fe-Mn-Si-based shape memory alloys containing NbC. *Materials Transactions*, 47: 580-583 (2006).

Song, G.Q., Sun, Q.P. and Cherkaoui, M., Role of microstructures in the thermomechanical behavior of SMA composites. *Journal of Engineering Materials and Technology*, 121: 86-92 (1999).

Tao X.Y. and Phillips D.V., A simplified isotropic damage model for concrete under bi-axial stress

states. *Cement and Concrete Composites* , 27: 716-726 (2005).

7. Tables

Table 1. Material properties of the SMA fibers (Panoskaltsis et al. (2004)).

Property	Value
E_A	1500 MPa
E_M	500 MPa
ν_A	0.3
ν_M	0.3
m	1
α	$5 \times 10^{-6}/°\text{C}$
C_A	1 MPa/°C
C_M	1 MPa/°C
ϵ_L	0.1
A_s	90 °C
A_f	130 °C
M_s	70 °C
M_f	10 °C
ϵ^0_{11}	0.08168
ϵ^0_{22}	-0.04084
ϵ^0_{33}	-0.04084

α is a coefficient of thermal expansion.

Table 2. Material properties of the concrete matrix (Tao and Phillips (2005)).

Property	Value
E	31.8 GPa
ν	0.18
α	$10 \times 10^{-6}/°\text{C}$
a_t	7000 MPa^{-1}
a_c	29 MPa^{-1}
b_t	1.1
b_c	0.94
Y^0_t	1.9 $\times 10^{-4}$ MPa
Y^0_c	3 $\times 10^{-4}$ MPa
c	2 MPa^{-1}
d	0.7 MPa^{-1}

α is a coefficient of thermal expansion.

Figure Captions

Fig. 1: One dimensional loading-unloading behavior for (a) $M_s < T < A_s$ and (b) $A_s < T < A_f$.

Fig. 2: One dimensional behavior for (a) uniaxial tension and (b) uniaxial compression.

Fig. 3: (a) A multiphase composite with doubly-periodic microstructures defined with respect to global coordinates (x_2, x_3). (b) The repeating unit cell is represented with respect to local coordinates (y_2, y_3). It is divided into N_β and N_γ subcells, in the y_2 and y_3 directions, respectively. (c) A characteristic subcell $(\beta\gamma)$ with local coordinates $\bar{y}_2^{(\beta)}$ and $\bar{y}_3^{(\gamma)}$ whose origin is located at its center.

Fig. 4: (a) Activated SMA fibers (oriented in the x_1-direction) embedded in a concrete matrix. The shapes of fibers are: (b) circle, (c) ring and (d) U-shaped.

Fig. 5: Effect of the shape of the SMA fibers on the behavior of the prestressed concrete: (a) Thermal expansion is not considered. (b) Thermal expansion is considered.

Fig. 6: (a) Effect of activation on the behavior of the prestressed concrete. (b) The ratio of the steady state axial stress $\bar{\sigma}_{ss}$ and the steady state axial stress in a SMA/concrete composite with no prestressing $\bar{\sigma}_{np}$ versus the martensite fraction ξ for different values of temperature deviations.

Fig. 7: Effect of fibers volume fraction v_f on the behavior of the prestressed concrete.

Fig. 8: Effect of activation temperature deviations on the transverse response of a prestressed concrete.

Fig. 9: Effect of fibers volume fraction v_f on the transverse response of a prestressed concrete.

Fig. 10: Effect of residual strains orientation on the response of a prestressed concrete. A square-shape SMA fiber is considered for three different orientations.

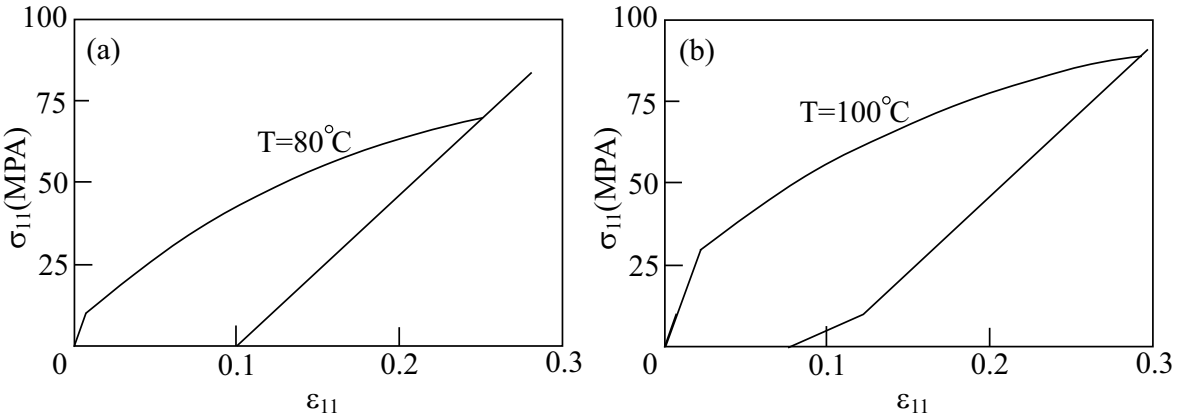
100
(a)
75
T=80°C
σ11(MPA)
50
25
0
0.1
0.2
0.3
ε11
100
(b)
75
T=100°C
σ11(MPA)
50
25
0
0.1
0.2
0.3
ε11

Fig.1

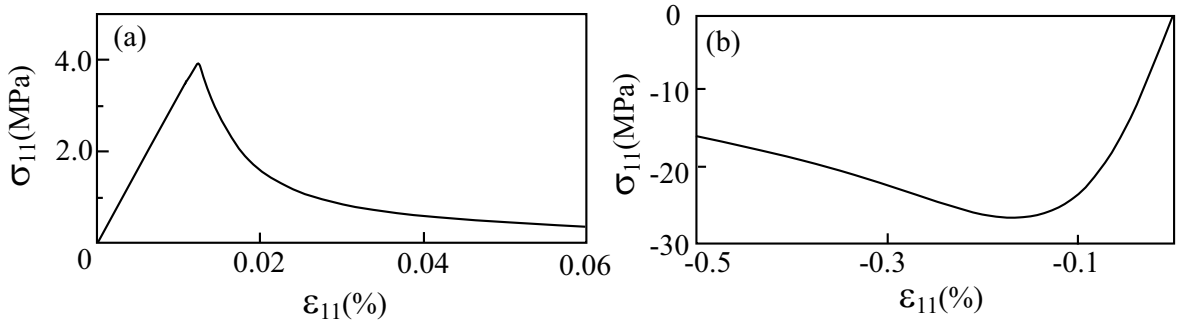

Fig. 2

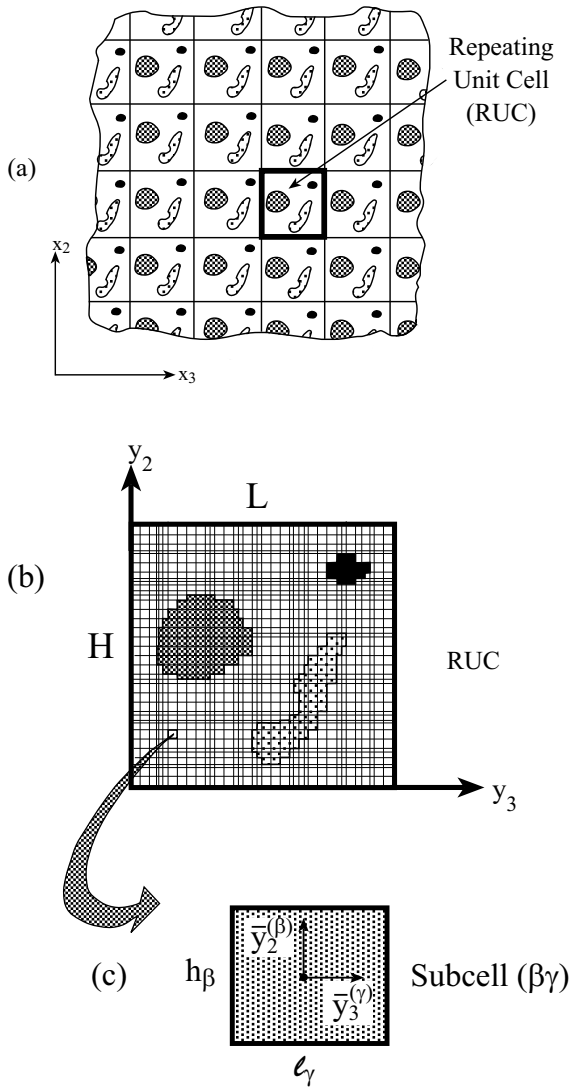

Fig. 3

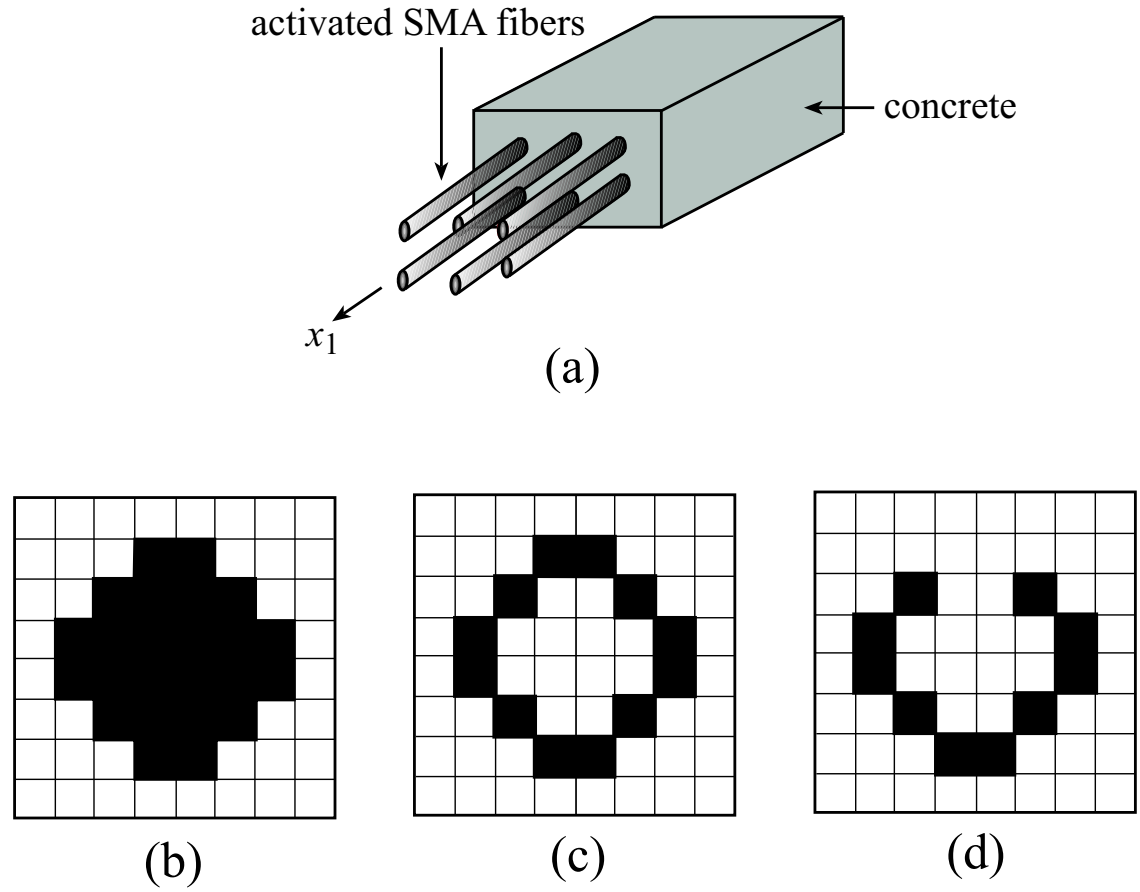

Fig.4

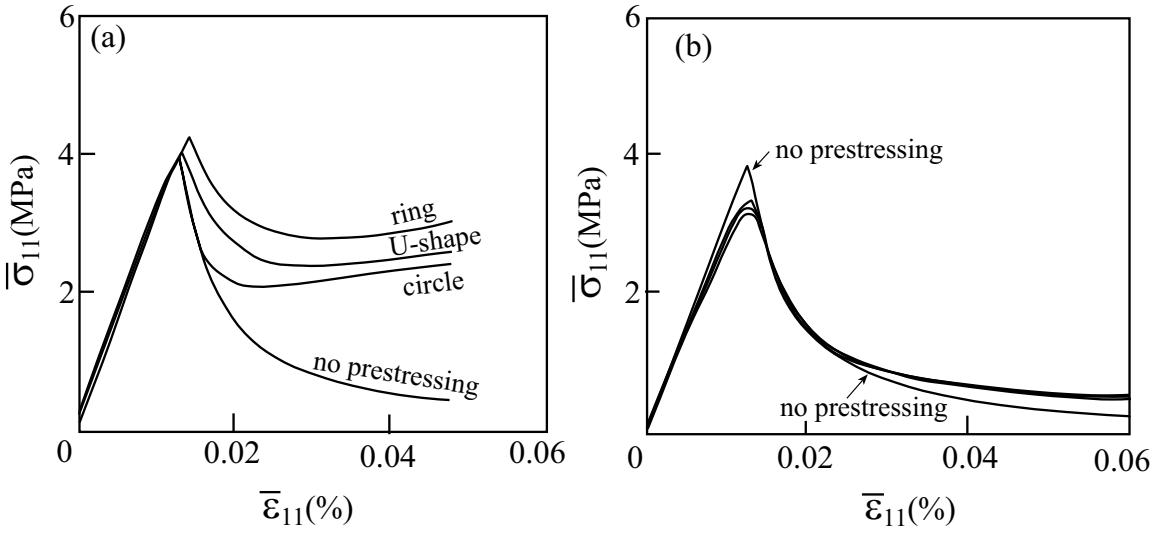
(a)
6
4
2
0
0.02
0.04
0.06
$\overline{\sigma}_{11}$(MPa)
$\overline{\varepsilon}_{11}$(%)
ring
U-shape
circle
no prestressing
(b)
6
4
2
0
0.02
0.04
0.06
$\overline{\sigma}_{11}$(MPa)
$\overline{\varepsilon}_{11}$(%)
no prestressing
no prestressing

Fig. 5

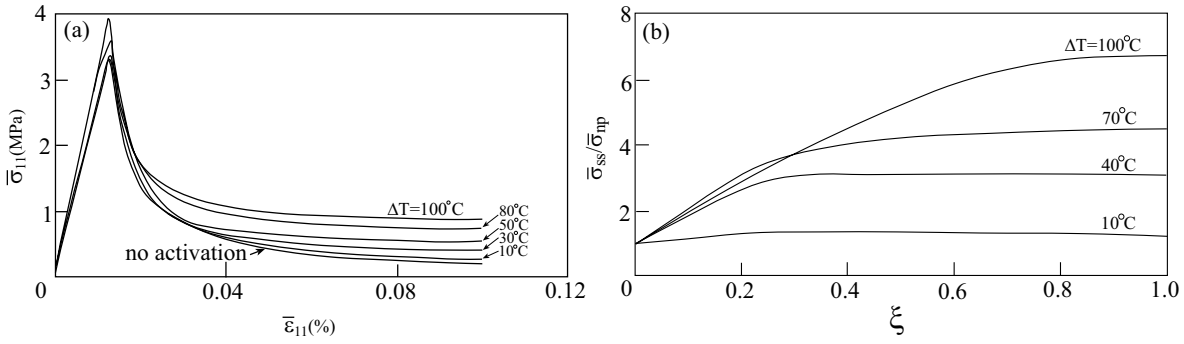
(a)
$\overline{\sigma}_{11}$(MPa)
$\overline{\varepsilon}_{11}$(%)
ΔT=100°C
80°C
50°C
30°C
10°C
no activation
0
0.04
0.08
0.12
1
2
3
4
(b)
$\overline{\sigma}_{ss}/\overline{\sigma}_{np}$
ξ
ΔT=100°C
70°C
40°C
10°C
0.2
0.4
0.6
0.8
1.0
6
8

Fig. 6

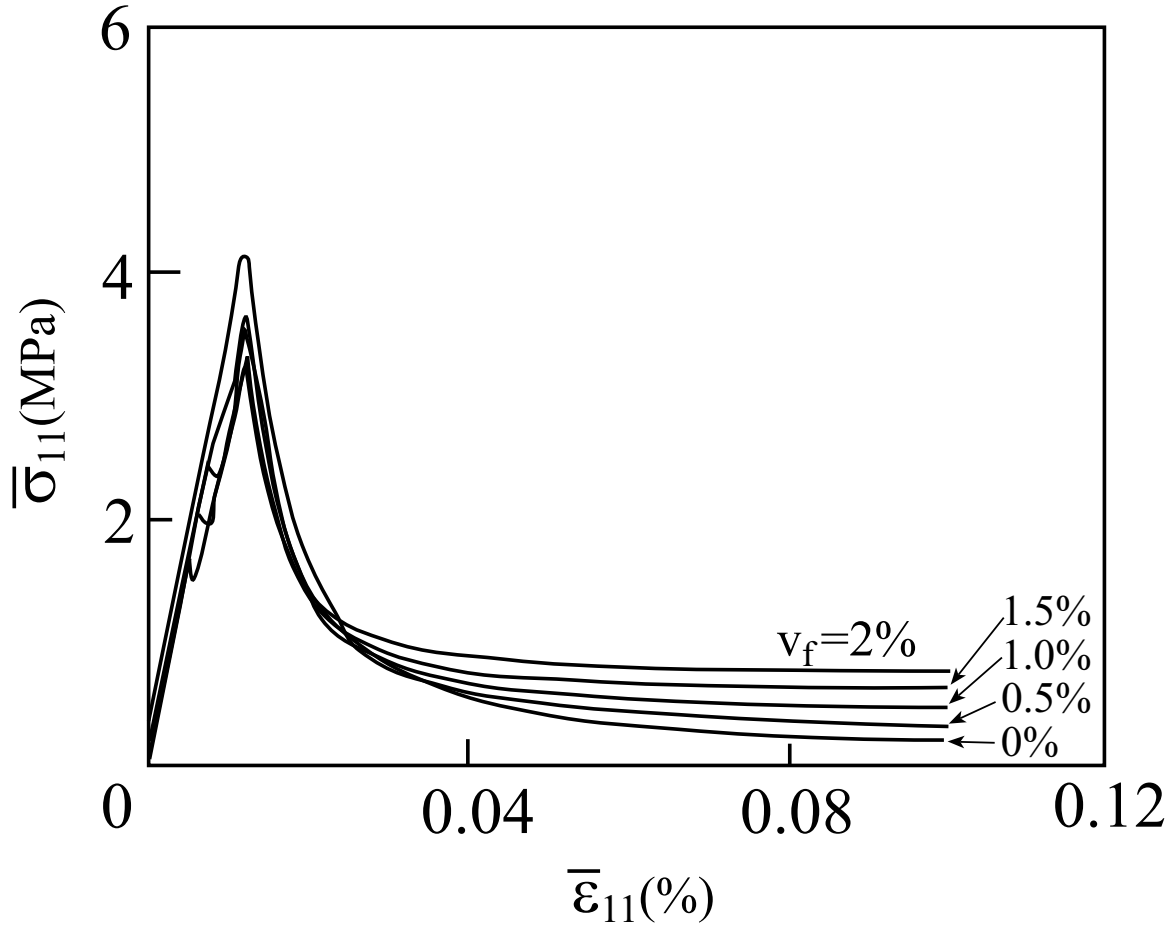
6
4
2
0
0.04
0.08
0.12
$\overline{\sigma}_{11}$(MPa)
$\overline{\varepsilon}_{11}$(%)
v_f=2%
1.5%
1.0%
0.5%
0%

Fig. 7

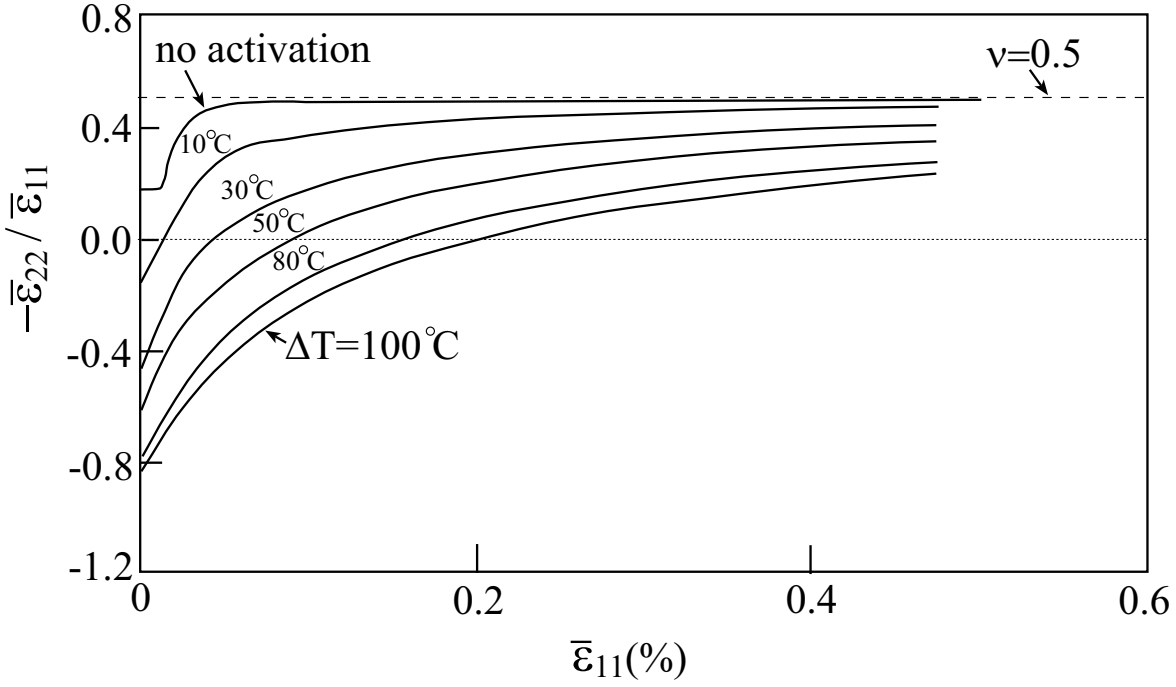
0.8
0.4
0.0
-0.4
-0.8
-1.2
0
0.2
0.4
0.6
no activation
ν=0.5
10℃
30℃
50℃
80℃
ΔT=100℃
$-\bar{\varepsilon}_{22} / \bar{\varepsilon}_{11}$
$\bar{\varepsilon}_{11}(\%)$

Fig.8

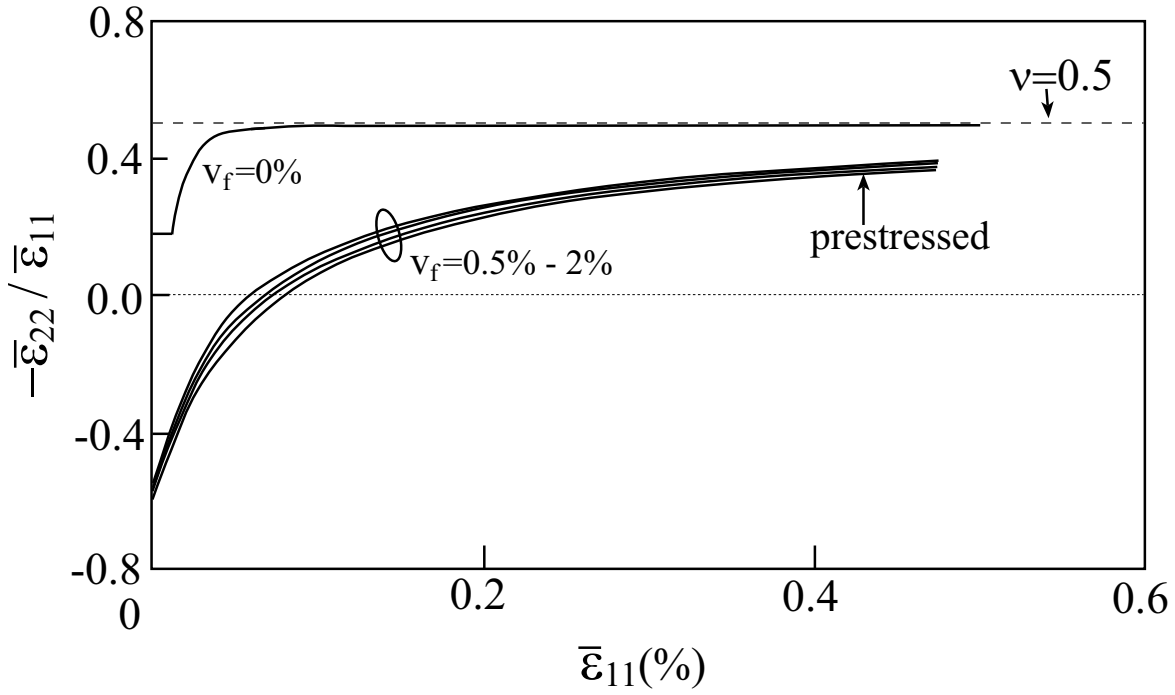

Fig.9

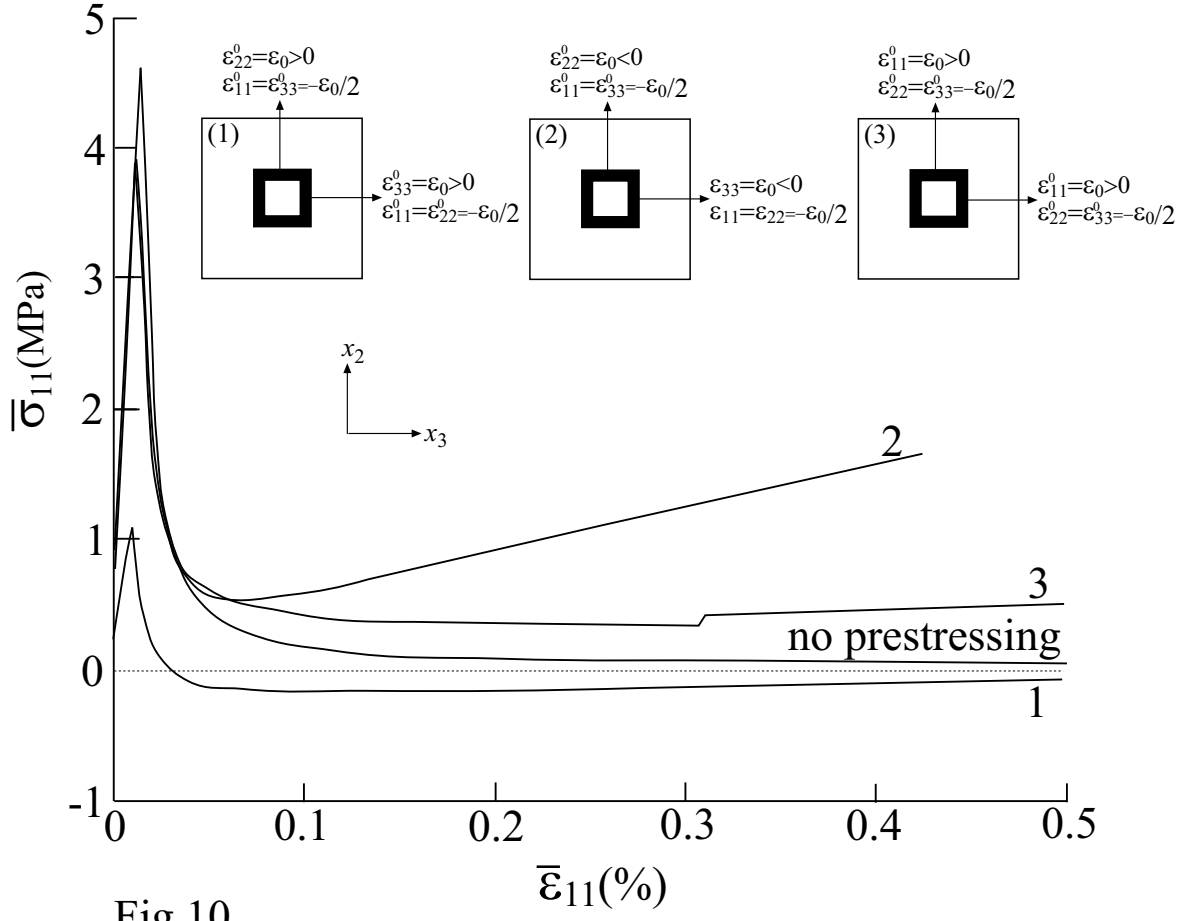
$\varepsilon^0_{22}=\varepsilon_0>0$
$\varepsilon^0_{11}=\varepsilon^0_{33}=-\varepsilon_0/2$
(1)
$\varepsilon^0_{33}=\varepsilon_0>0$
$\varepsilon^0_{11}=\varepsilon^0_{22}=-\varepsilon_0/2$
$\varepsilon^0_{22}=\varepsilon_0<0$
$\varepsilon^0_{11}=\varepsilon^0_{33}=-\varepsilon_0/2$
(2)
$\varepsilon_{33}=\varepsilon_0<0$
$\varepsilon_{11}=\varepsilon_{22}=-\varepsilon_0/2$
$\varepsilon^0_{11}=\varepsilon_0>0$
$\varepsilon^0_{22}=\varepsilon^0_{33}=-\varepsilon_0/2$
(3)
$\varepsilon^0_{11}=\varepsilon_0>0$
$\varepsilon^0_{22}=\varepsilon^0_{33}=-\varepsilon_0/2$
x_2
x_3
$\overline{\sigma}_{11}$(MPa)
$\overline{\varepsilon}_{11}$(%)
2
3
no prestressing
1
5
4
3
2
1
0
-1
0
0.1
0.2
0.3
0.4
0.5

Fig.10